

Part III: RESULTS AND DISCUSSION**NON-ERGODIC PROBABILISTIC SEISMIC HAZARD METHODOLOGY USING PHYSICS-BASED GROUND MOTION PREDICTION THE CASE OF L'AQUILA, ITALY**JEDIDIAH JOEL AGUIRRE^{1,2}, BRUNO RUBINO¹, MAURIZIO VASSALLO³, GIUSEPPE DI GIULIO³ AND FRANCESCO VISINI⁴¹Università Degli Studi Dell'Aquila 67100 L'Aquila, Italy²University of the Philippines 4031 Los Baños, Laguna, Philippines³Istituto Nazionale di Geofisica e Vulcanologia – Sezione dell'Aquila 67100 L'Aquila, Italy⁴Istituto Nazionale di Geofisica e Vulcanologia – Sezione di Pisa 56125 Pisa, Italy

(received: 4 January 2020; revised: 9 February 2020; accepted: 15 March 2020; published online: 1 April 2020)

DOI: https://doi.org/10.34808/tq2020/24.2/a_part3**11. Results and Discussion****11.1. Model Used and Summary of Values for Seismic Sources**

Table 6 shows the earthquake recurrence source model used and the range of values of magnitude and activity rates obtained from the attached file in the link provided by Valentini et al. [24] for each of the 28 seismic sources identified in this study. It should be noted that some seismic sources in this study were not obtained from Valentini et al. [24], and so the author used the FiSH code to determine the activity rates of these sources. The fault data of these sources were obtained from the attached file in the link provided by Valentini et al. [25].

A total of 325 scenarios were considered in this study which was determined by counting the magnitude occurrences in all seismic sources. A binning of 0.1 was used to generate the magnitude PDF. As mentioned before in Subsection 5.1.1, the following was employed for choosing a suitable earthquake recurrence model for each fault: a) the TGR model was used for fault sources that had no data regarding the last earthquake occurrence from Table 2; b) the TGR model was used in the case that the active fault sources had earthquake associations based on Table 3, if there was at least one earthquake having a magnitude lower than magnitude range for the CHBPT model; c) otherwise, the CHBPT was used. Based on Table 6, there are 15 seismic sources that were modeled as CHBPT, while the remaining 13 sources were modeled as TGR since most of these sources were not considered by Valentini et al. [24], or the seismic source had no recording of past earthquakes based on Table 3.

For the sources modeled with TGR, the minimum magnitude was set to 5.5, while the maximum magnitude was the value from Table 5 which was obtained using the FiSH Code as per data extracted from Valentini et al. [24]. For sources modeled with CHBPT, the minimum magnitude was set to $M_{max} - sDM_{max}$, while the maximum magnitude was set to $M_{max} + sDM_{max}$. As a result, the maximum magnitude considered in this study, which can be seen in Table 6, was 7.1 from the Fucino fault, followed by the Gran Sasso and Mount Bevore-Mount Bove faults with magnitude 7.0.

The activity rate is the reciprocal of the mean recurrence time of earthquakes and has units of earthquakes per year. It follows from Table 2 that the Maiella fault has the highest range of activity rates, with 2.89×10^{-4} to 2.89×10^{-3} earthquakes/year, while the Mount Vettore — Mount Bove fault has the

Table 6. The recurrence model used and the magnitude and activity rate ranges from each seismic source [25, 24]

*TGR — Truncated Gutenberg-Richter, CHBPT — Characteristic Brown Passage Time

ID	Source Name	Source Model	Magnitude		Activity Rates (eq/year)	
			Min	Max	Min	Max
1	Barrea	TGR	5.5	6.3	1.03E-04	6.48E-04
2	Campo Felice Ovindoli	CHBPT	6.4	6.8	2.15E-04	3.54E-04
3	Carsoli	TGR	5.5	6.4	1.33E-04	1.06E-03
4	Cascia Cittareale	TGR	5.5	6.5	1.21E-03	1.21E-04
5	Cassino	TGR	5.5	6.5	5.80E-05	5.80E-04
6	Colfiorito	TGR	5.5	6.4	9.27E-05	7.36E-04
7	Fucino	CHBPT	6.5	7.1	4.42E-06	7.28E-06
8	Gran Sasso	CHBPT	6.4	7	5.39E-05	8.89E-05
9	Leonessa	TGR	5.5	6.2	1.88E-04	9.44E-04
10	Liri	TGR	5.5	6.8	4.81E-05	9.61E-04
11	Maiella	TGR	5.5	6.5	2.89E-04	2.89E-03
12	Marsicano	CHBPT	6.3	6.7	1.72E-04	2.83E-04
13	Middle Aternum Valley	CHBPT	6.4	6.8	9.44E-05	1.56E-04
14	Monte reale	CHBPT	6	6.6	1.20E-04	1.98E-04
15	Mount Gorzano	TGR	5.5	6.6	1.20E-04	1.51E-03
16	Mount Vettore - Mount Bove	CHBPT	6.4	7	4.93E-12	8.13E-12
17	Nottoria Preci	TGR	5.5	6.6	9.20E-05	1.16E-03
18	Paganica	CHBPT	6.3	6.7	5.13E-12	8.46E-12
19	Pizzalto C. Miglia	CHBPT	6.1	6.7	7.04E-05	1.16E-04
20	Pizzoli-Pettino	CHBPT	6.3	6.7	1.32E-04	2.18E-04
21	Rieti	CHBPT	6	6.6	7.80E-05	1.29E-04
22	Salto Valley	CHBPT	6.3	6.7	1.19E-04	1.96E-04
23	Sella di Corno	TGR	5.5	6.5	1.11E-04	1.11E-03
24	Sora	CHBPT	6.2	6.6	3.12E-05	5.14E-05
25	Sulmona	CHBPT	6.3	6.7	3.12E-05	5.14E-05
26	Umbrea Valley N	TGR	5.5	6.3	3.67E-05	2.31E-04
27	Umbrea Valley S	TGR	5.5	6.2	5.37E-05	2.69E-04
28	Velino	CHBPT	5.8	6.4	2.40E-04	3.96E-04

smallest ranges of activity rates, ranging from 4.93×10^{-12} to 8.13×10^{-12} earthquakes/year. This means that the Maiella fault is the biggest contributor to the seismic hazard in terms of the earthquake occurrence while Mount Vettore — Mount Bove is the smallest contributor to the seismic hazard. However, it should be noted that this is not conclusive for the overall seismic hazard, since this applies to the earthquake occurrence only, and does not include other factors such

as magnitude, distance, and the predicted PGA. A total of 2800 distances were generated in this study by subdividing each seismic source into 100 equal parts, and the centroids of these areas were calculated using ArcGIS Pro. The resulting distances were grouped into 10 bins per source, and the probabilities of occurrence were calculated by dividing the frequency per bin divided by 100. Table 6 shows the range of source-to-site distances (in kilometers) of the 28 seismic sources to L'Aquila. The distance PDFs can be found in Appendix B to this paper.

Table 7 shows that the Paganica fault is the nearest seismic source which can affect L'Aquila, with distances ranging from 1.64 to 21.36 km, followed by the Pizzoli-Pettino fault with distances ranging from 4.61 to 29.36 km. In 2009, the Paganica fault caused catastrophic damage to L'Aquila due to the Mw 6.3 earthquake it produced. Hence, this fault can pose a threat to the city of L'Aquila anytime without much predictability on the fault's rupture. Table 7 also shows that the farthest fault is the Umbrea Valley Fault North segment which is located ranging from 98.23 to 126.71 km. Therefore, in terms of contribution to the overall seismic hazard, the Paganica and Umbrea Valley North faults are the highest and lowest contributors to the city of L'Aquila. Since there are fault sources that are located too far away from the city, only a maximum distance of 100 km was considered for these sources since we are only concerned with such sources which can significantly contribute to the overall seismic hazard.

It should be noted here that the frequencies of the distances that were considered for the probability computations were those obtained within a 100 km radius from L'Aquila, and their frequencies were divided by 100, and not by the number of total distances that fell within 100 km, since the probability of occurrence of a certain distance within the seismic source is the subject of the source-to-site uncertainty within the source. Also, these distances were the lengths of wave propagations required for the PGA Prediction.

The resulting probability of occurrence of the distance per magnitude occurrence is the resulting probability of exceedance per rupture scenario in (93).

12. Peak Ground Acceleration Prediction

As mentioned before in Subsection 5.1.1, two actual ground motions coming from L'Aquila and Central Italy events were used to determine the grid spacing to be used for this study. The soil types considered were site class B for the former and site class A for the latter, with the former transformed into site class A by dividing the amplification factors according to the National Earthquake Hazards Reduction Program (NEHRP) Seismic Provisions [49] applicable for short period responses.

Table 8 shows the details of the two ground motions used from the Engineering Strong Ground Motion [46]. For the L'Aquila earthquake, the PGA recorded at the seismogram with the epicenter at 4.9 km is $0.664g$ with site class B, which is multiplied by 0.8 to match the site class A as per the NEHRP Seismic Provisions. For the Central Italy earthquake, the PGA recorded at the seismogram

Table 7. Source-to-site distances obtained for the City of L'Aquila. The maximum distance is limited to 100 km

*TGR — Truncated Guttenburg-Richter, CHBPT — Characteristic Brown Passage Time

ID	Source Name	Source-to-Site Distances (km)	
		Min	Max
1	Barrea	88.14	105.67
2	Campo Felice Ovindoli	8.36	31.34
3	Carsoli	39.25	49.13
4	Cascia Cittareale	38.93	62.36
5	Cassino	97.25	123.75
6	Colfiorito	81.85	128.59
7	Fucino	25.32	59.05
8	GranSasso	8.32	41.12
9	Leonessa	46.32	63.19
10	Liri	40.03	68.07
11	Maiella	69.26	85.38
12	Marsicano	62.76	87.22
13	Middle Aternum Valley	18.83	48.49
14	Monte Reale	14.77	33.56
15	Mount Gorzano	12.57	42.25
16	Mount Vettore Mount Bove	45.25	79.64
17	Nottoria Preci	47.7	75.99
18	Paganica	1.64	21.36
19	Pizzalto C. Miglia	75.72	92.34
20	Pizzoli-Pettino	4.61	29.36
21	Rieti	47.8	66.17
22	Salto Valley	25.2	48.27
23	Sella di Corno	20.99	44.86
24	Sora	73.16	90.23
25	Sulmona	46.36	76.49
26	Umbra Valley N	98.23	126.71
27	Umbra Valley S	78.44	98.79
28	Velino	23.00	32.19

is $0.577g$ with the epicenter at 18.6 km. By trial and error, the appropriate grid spacings to be used are 24 and 19.8 m, say 20 m, for the sake of conservatism.

Using a uniform spacing of 20 m, the PGAs were estimated with different possible magnitude-distance pairs in each seismic source identified in this study. A total of 2013 simulations were performed across all seismic sources. Table 9 summarizes the PGA obtained in each seismic source.

Table 8. Attributes of the 2009 L'Aquila and 2016 Central Italy Earthquakes from the Engineering Strong Ground Motion [46]

Attributes	L'Aquila Event	Central Italy Event
Event ID	IT-2009-09	EMSC-20161030_0000029
Date	06042009	30102016
M_w	6.1	6.5
Station Code	4A.MI05	IT.ACC
Latitude	42.626	13.242
Longitude	42.28947	13.525526
PGA (g)	0.557	0.664
Soil Type	B	A

It follows from Table 9 that the minimum PGAs were observed in the Cassino and Umbrea Valley North segment faults with a value of $0.114g$, while the maximum was observed in the Paganica fault with a value of $2.160g$. These extreme values were expected to be in these seismic sources due to the combinations of the magnitude-distance for which they belong, and the model used to account for the recurrence of earthquakes in these sources. For Cassino and the Umbrea Valley North segment, the TGR model was used which considers a minimum magnitude of 5.5, and the distances of these faults from L'Aquila were 97.25 km and 98.23 km, respectively at the nearest, thus making the magnitude-distance pair of M_w 5.5, 100 km produce the minimum value in this study. For Paganica, the CHBPT model was used which utilized its maximum magnitude of 6.5 defined by this study plus one standard deviation of 0.2 while the nearest distance from the causative fault is 1.64 km, making the magnitude-distance pair produce the maximum value in this study.

12.1. Peak Ground Acceleration vs. Fault Length

The fault length affects the two parameters required for simulation of earthquakes, namely the maximum magnitude in each fault and the rupture time t_r . It is obvious from (83) that an increase in the fault length increases the maximum magnitude to be considered in a seismic source, and the moment magnitude is directly related to the seismic moment. The higher the fault length, the higher the seismic moment and so the higher the stress drop in a fault, which is directly related to the PGA. On the other hand, the rupture time, as defined in Subsection 3.2.1 of this paper, is directly proportional to the fault rupture length as well, which directly influences the variation in the stress drop in the fault as presented in the extended friction law model defined in this study. Table 10 shows the variation of some selected PGA values as a function of the fault length, considering (more or less) the same length of propagation (or distances) and the same magnitudes of occurrences.

In Table 10 it can be observed that the PGA does not vary that much across all the distances, and the variation is significant only up to the order of magnitude

Table 9. Predicted PGA in each seismic source

ID	Source Name	Predicted PGA (in g's)	
		Min	Max
1	Barrea	0.117	0.215
2	Campo Felice-Ovindoli	0.387	0.991
3	Carsoli	0.163	0.345
4	Cascia-Cittareale	0.143	0.373
5	Cassino	0.114	0.236
6	Colfiorito	0.115	0.244
7	Fucino	0.303	0.662
8	Gran Sasso	0.338	1.159
9	Leonessa	0.143	0.275
10	Liri	0.137	0.457
11	Maiella	0.123	0.280
12	Marsicano	0.213	0.336
13	Middle Aternum Valley	0.310	0.667
14	Montereale	0.280	0.651
15	Mount Gorzano	0.173	0.700
16	Mount Vettore-Mount Bove	0.242	0.497
17	Nottoria-Preci	0.122	0.342
18	Paganica	0.452	2.160
19	Pizzalto-Cinque Miglia	0.181	0.310
20	Pizzoli-Pettino	0.372	1.248
21	Rieti	0.199	0.362
22	Salto Valley	0.286	0.531
23	Sella di Corno	0.168	0.508
24	Sora	0.198	0.294
25	Sulmona	0.229	0.392
26	Umbrea Valley N	0.114	0.203
27	Umbrea Valley S	0.115	0.212
28	Velino	0.247	0.450

of 10^{-3} to 10^{-2} . As far as ocular observations are concerned, the values of PGA do not vary that much in relation to the fault length, and so regardless of the fault length, simulations of the fault rupture can be made to estimate the ground motion.

Given that the PGA does not vary that much in length of a fault rupture, one can simulate ground motions which can be used to determine the effect of site classes (soil type), epicentral and/or hypocentral distances, and grid spacing. These are not considered in this paper as they are beyond the scope of this study.

Table 10. Variation of PGA as a function of Fault Rupture Length. Each sub-table are grouped according to same magnitude of occurrence and more or less the same length of propagation. The fault length (L) is compared against the PGA given the distance and magintude.

L (km)	26.5	28.7	L (km)	21.5	23.7	L (km)	26.5	28.7
M/R	8.32	8.36	M/R	10.11	10.41	M/R	19.17	19.9
6.4	0.741	0.75	6.3	0.646	0.632	6.4	0.494	0.483
6.5	0.797	0.807	6.4	0.649	0.68	6.5	0.531	0.520
6.6	0.857	0.867	6.5	0.746	0.731	6.6	0.571	0.558
6.7	0.922	0.933	6.6	0.802	0.786	6.7	0.614	0.600
6.8	0.991	1.003	6.7	0.863	0.846	6.8	0.660	0.646

L (km)	21.5	23.7	L (km)	11.5	23.1	L (km)	11.5	23.1
M/R	21.11	21.362	M/R	23	23.64	M/R	26.06	26.29
6.3	0.434	0.452	5.8	0.291	0.288	5.8	26.06	26.29
6.4	0.467	0.485	5.9	0.313	0.31	5.9	0.274	0.273
6.5	0.502	0.522	6.0	0.336	0.333	6.0	0.294	0.293
6.6	0.540	0.561	6.1	0.362	0.358	6.1	0.316	0.315
6.7	0.581	0.603	6.2	0.389	0.385	6.2	0.375	0.364
			6.3	0.419	0.414	6.3	0.393	0.392
			6.4	0.450	0.445	6.4	0.423	0.421

13. Seismic Hazard Curves

Figure 22 shows the resulting seismic hazard curves for the city of L’Aquila which present the total hazard (topmost curve) and individual hazard curves contributed by each of the seismic sources identified in this study. This figure shows that Maiella, Mount Gorzano and Leonessa contributed the highest hazard rates in smaller values of PGA and Mount Vetorre — Mount Bove contributed the least. On the other hand, Campo Felice-Ovindoli, Pizzoli-Pettino, Fucino, Gran Sasso, and the Paganica Fault contributed the most hazard rates in higher values of PGA while other faults did not contribute to the hazard rates of higher PGA. Specifically, it was only the Paganica Fault that contributed to the hazard in L’Aquila in PGA values greater than 1.30g. Higher hazard values for smaller values of PGA are evident to seismic sources which are modeled with the TGR recurrence model and those that are very far from L’Aquila. It has been mentioned before that Maiella has the highest rates, and hence contributes to the seismic hazard at small values of PGA. The Paganica Fault, the closest fault in L’Aquila, has very small hazard rates but produces the highest PGA values due to the small distance — high magnitude combinations.

The resulting hazard curve has an abrupt change in the slope at PGA equal to 0.70g as shown in Figure 22. This can be attributed to a decrease in the number

Table 11. Table 10 — continued

L (km)	26.5	28.7	L (km)	34	22.6	42.5
M/R	31.34	31.47	M/R	52.89	53.05	53.22
6.4	0.387	0.384	6.3	0.298	0.295	0.300
6.5	0.417	0.413	6.4	0.321	0.317	0.319
6.6	0.448	0.444	6.5	0.345	0.341	0.343
6.7	0.482	0.478	6.6	0.371	0.366	0.369
6.8	0.518	0.514				

L (km)	22.6	42.5	34
M/R	59.75	59.82	60.54
6.4	0.278	0.282	0.278
6.5	0.299	0.300	0.299
6.6	0.321	0.322	0.322
6.7	0.345	0.347	0.346

L (km)	17.4	24.6	28.6	45
M/R	100	100	100	100
5.5	0.127	0.115	0.114	0.115
5.6	0.129	0.121	0.121	0.124
5.7	0.136	0.131	0.131	0.133
5.8	0.147	0.140	0.140	0.143
5.9	0.155	0.151	0.151	0.154
6.0	0.162	0.162	0.162	0.165
6.1	0.174	0.174	0.174	0.178
6.2	0.187	0.187	0.187	0.191

L (km)	18	24	24	18	24	18
M/R	80.7	81.26	84.95	85.23	92.01	92.34
6.1	0.194	0.193	0.189	0.189	0.182	0.181
6.2	0.208	0.208	0.203	0.203	0.195	0.195

of the seismic sources that contribute only to the small value of PGA. In fact, only the five seismic sources mentioned above which contributed greatly to the seismic hazard corresponding to higher values of PGA, say above $0.70g$, comprise that portion of the seismic hazard curve where the slope changes abruptly. Lastly, the curve changed abruptly again at a PGA value of $1.30g$, for it is attributed solely due to the Paganica Fault.

Figure 23 shows a comparison of the hazard curve in this study with the work of Valentini et al. [24]. It follows from the figure that the hazard curve

produced in this study is higher than the hazard curve in Valentini et al. [24], which can be attributed to the higher values of PGA that are simulated by solving the elastodynamic equation. On the other hand, the hazard curve of Valentini et al. [24] is higher than that the hazard curve of this study, which can be attributed to the smaller number of seismic sources considered in this study. The hazard curve of Valentini et al. [24] considered both fault sources and distributed sources, and therefore this study can be further improved by considering the distributed sources as well. For the portion of the hazard curve which is higher than that of Valentini et al. [24], the grid spacing used in the simulation can be varied depending on the distance from the fault. Also, the fault parameters in relation to the PGA prediction can be calibrated using other soil types and other ground motion data available in the Engineering Strong Motion Database.

14. Application of PSHA to Seismic Design

This hazard curve can be used to determine the feasible ground motion properties that a future earthquake can produce in terms of its return period. With the given mean annual rate of exceedance, one can obtain the return period using its reciprocal. As mentioned before in Subsection 5.1.1, the seismic design of structures requires a minimum value of PGA with a probability of exceedance of 10% in 50 years of the exposure time, and this corresponds to a return period of 475 years or 0.00202 earthquakes per year. Also, for a higher hazard consideration, a PGA value having a probability of exceedance of 2% can be used, which has a return period of 2475 years or a hazard rate of 4.04E-04. Interpolating these values from the constructed hazard curve in Figure 5.1 enables an engineer to construct the elastic design spectrum. Figure 24 shows the PGA values corresponding to 10% and 2% probability of exceedances in 50 years' exposure time, and Figure 5.4 shows the elastic design spectra corresponding to the probability of exceedances.

15. Summary and Conclusion

A non-ergodic probabilistic seismic hazard analysis (PSHA) was carried out in the study area of the city of L'Aquila, Italy due to its proximity to several active faults in Central Italy and past seismicity leading to catastrophic damage in the city brought by the 2009 L'Aquila earthquake. This non-ergodic approach was taken by solving the Elastodynamic Equation coupled with the Hooke's Law, both of which form a system of Hyperbolic equations, which is another form of the Elastic Wave Equation.

A total of 28 seismic sources were identified in this study located within a 100 km radius from the city, and a map was produced to show all the seismic sources using ArcGIS. To characterize the variation in source-to-site distances, each seismic source was subdivided into 100 equal areas, and the centroids of each resulting areas were calculated using ArcGIS, after which the histograms with 10 bins each were created to be used for the probability of the exceedance calculations. Each of the seismic sources was characterized by its fault geometric

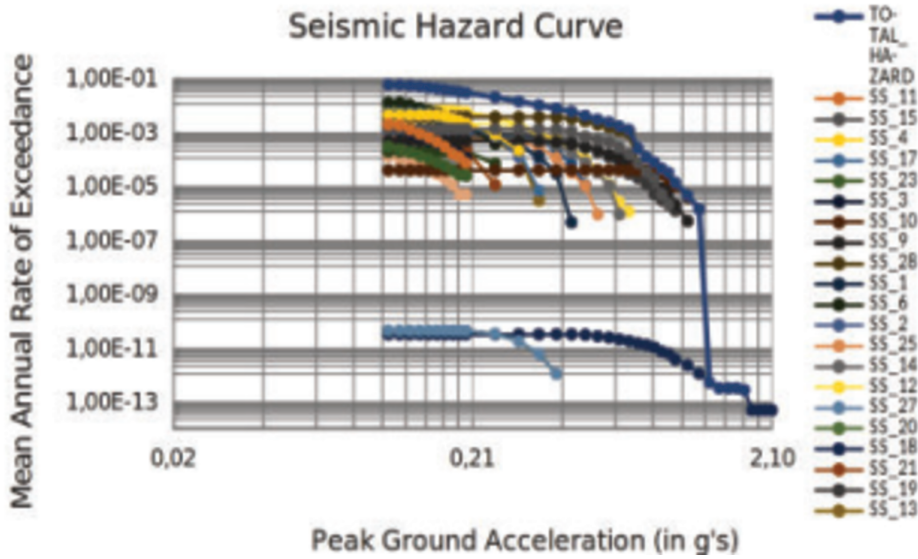


Figure 22. Seismic Hazard Curve for the City of L'Aquila, Italy

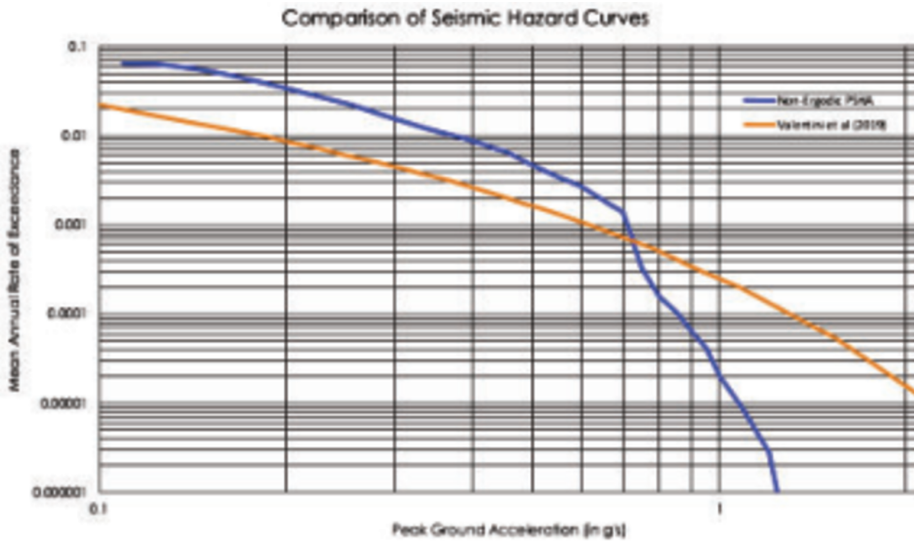


Figure 23. Comparison of the hazard curve in this study with the hazard curve of Valentini et al. [24]

properties such as length, dip, slip rates, seismogenic thickness, the observed magnitude of occurrence, and the last year of occurrence, all of which were obtained from Valentini et al. [25] and Valentini et al. [24]. To model the recurrence of earthquakes in each source, past seismicity in the form of the paleoseismic activity and historical earthquakes was extracted from Valentini et al. [24] as well, and the activity rates were calculated using the FiSH Code by Pace, Visini,

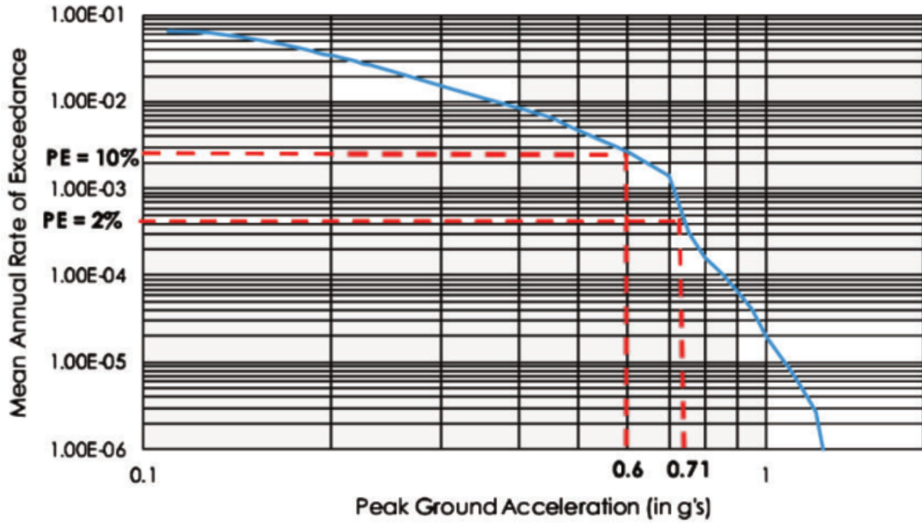


Figure 24. PGA values corresponding to 10% and 2% probability of exceedances

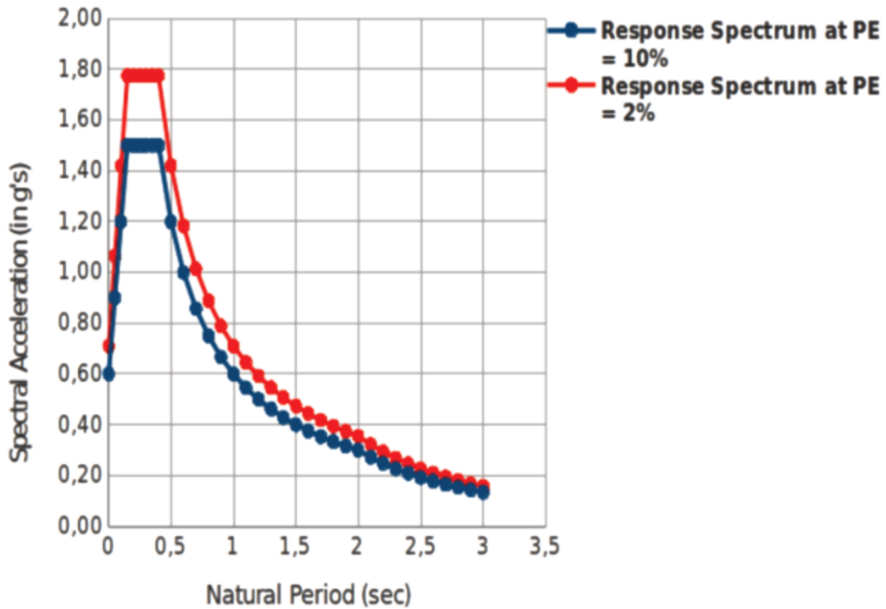


Figure 25. Elastic Design Spectrum corresponding to 10% and 2% probability of exceedances

and Peruzza [41]. The maximum magnitude was calculated in each fault by the criteria set forth in Subsection 5.1. Two recurrence models were employed in this study; the Truncated Gutenberg-Richter (TGR) and Characteristic Brownian Passage Time (CHBPT) models, as set forth by Subsection 5.1.1.

After the data had been extracted from Valentini et al. [25] and Valentini et al. [24], the seismic moments, fracture energy, stress drop were computed using a set of empirical equations from Causse et al. [31]. Then, a physics-based ground motion prediction by solving the Elastodynamic Equation and the Hooke's Law was employed by applying the extended friction law model as a boundary condition for pressure in each fault, and synthetic seismograms were produced in all the distances calculated in ArcGIS and the magnitude of occurrences in each fault source. The grid spacing was chosen by considering the actual ground motions obtained from the 2009 L'Aquila and 2016 Central Italy earthquakes. The earth is modeled as a 1-D model which is according to the PREM Model, for which the density and the S-wave velocity was obtained considering the seismogenic thickness of each fault. The peak ground accelerations (PGA) in each seismogram were obtained, and histograms of PGA were created in terms of frequency of distances to calculate the probability of exceedance of a PGA value given a reference PGA. Lastly, the hazard curve was calculated using the formulation by Tarbali et al. [19, 20]. The resulting hazard curve was compared to the hazard curve of Valentini et al. [24].

Based on the activity rates obtained, Maiella has the highest value which turns out to be one of the highest contributors to the overall seismic hazard considering the lower values of PGA, while Mount Vetorre — Mount Bevo has the lowest activity, followed by the Paganica Fault. In terms of proximity to the city of L'Aquila, Paganica is the nearest, while Umbrea Valley North Segment and Colfiorito are the farthest. The highest PGA values were obtained from Paganica due to its proximity to the fault and the high magnitude of occurrence, while the Umbrea Valley North Segment and Cassino produced the lowest PGA of all. Higher values of PGA resulted from the CHBPT recurrence model and proximity to the fault sources, while lower values of PGA resulted from the TGR recurrence model and longer lengths of wave propagations.

The PGA values did not vary too much considering the fault rupture length, which in turn is directly related to the rupture time, and therefore, a simulation of ground motions can be performed to determine the effect of site classes, epicentral or hypocentral distances, and grid spacing.

Maiella, Mount Gorzano, and Leonessa contributed the highest hazard rates in smaller values of PGA and Mount Vetore — Mount Bove contributed the least. On the other hand, the Campo Felice-Ovindoli, Pizzoli-Pettino, Fucino, Gran Sasso and Paganica Faults contributed the most hazard rates in higher values of PGA while other faults did not contribute to the hazard rates of higher PGA. The seismic hazard curve produced in this study is higher than that of Valentini et al. [24] for a PGA smaller than or equal to $0.70g$, while the opposite is true for PGA greater than $0.70g$. This can be attributed to the overestimation of PGA at larger distances, and thus can be resolved by varying the grid spacing given a certain length of propagation in order to decrease the hazard rate at lower values of PGA. On the other hand, to increase the hazard rates at higher PGA values,

it is recommended to include distributed sources in the seismic hazard analysis. Also, other parameters regarding the fault rupture can be calibrated using the actual ground motion data considering longer source-to-site distances.

As application to the seismic design, the PGA values corresponding to 10% and 2% probability of exceedance were obtained from the resulting hazard curve of this study, and the elastic design spectra considering these two probabilities of exceedances were constructed and can be readily used.

16. Recommendations

The researcher believes that the fault data and the past seismicity used in this study are robust, nonetheless, they still can be improved by updating the earthquake catalogue including the past seismicity in the case of new occurrences. Also, the available S-wave velocity and the rock density profile can be used to improve the estimation of the ground motion, instead of using constant values of S-wave velocity and density.

When it comes to the numerical simulation of earthquakes using the Finite Difference Method, different grid spacings must be employed by studying the appropriate grid spacing given a range of values of the length of propagation and the site class type, which depend on the shear wave velocity of the soil, since accelerometers were located on the surface of the soil and not on the bedrock. Also, the extended friction law can be improved by calibrating the initial dynamic stress value against the actual ground motion data. Another possibility is to incorporate the seismogenic thickness to consider the hypocentral distances instead of epicentral distances; this also opens a possibility of exploring the actual stresses in the fault as long as data regarding the unit weight and the presence of a water table and other factors affecting effective stresses can be obtained to improve the values used in the extended friction law. With the improvement of the seismic parameters to be used to simulate an earthquake, a 2D or even 3D Elastodynamic Equation can be used to predict the PGA on a site.

To improve the seismic hazard curve, distributed sources must be studied as well and incorporated into the seismic hazard to improve the hazard rates in PGA higher values. Also, a hybrid of hazard rates can be considered by contemplating a certain grid spacing for a certain distance, thus employing different grid spacings to avoid overestimation in the PGA.

As for other numerical methods to simulate earthquakes, the Finite Element Method is also a well-known method to solve the elastodynamic equation, which can be a better approximation than the Finite Differences. The use of Green Functions, a widely used method to produce synthetic seismograms, can also be utilized to estimate the PGA.

Acknowledgment

The main author would like to thank the University of the Philippines System through the Office of the Vice-President of Academic Affairs and the Uni-

versity of the Philippines Los Baños through the Office of the Vice-Chancellor of Academic Affairs and the Department of Civil Engineering for all the administrative and financial support received from them to make this study possible. Also, a special mention to INGV L'Aquila and Dr. Francesco Visini for the data used in this study.

REFERENCES

- [19] Tarbali K, Bradley B, Huang J, Polak V, Lagrava D, Motha J, and Bae S 2018 CYBERSHAKE NZ V179: New Zealand simulation-based probabilistic seismic hazard analysis, 16th European Conference on Earthquake Thessaloniki Engineering
- [20] Tarbali K, Bradley B, Huang J, Lee R, Lagrava D, Bae S, Polack V, Motha J, and Zhu M 2019 CYBERSHAKE NZ V185: New Zealand simulation-based probabilistic seismic hazard analysis, 2019 Pacific Conference on Earthquake Engineering - New Zealand Society for Earthquake Engineering
- [24] Valentini A, Pace B, Boncio P, Visini F, Pagliaroli A, and Pergalani F 2019 Definition of seismic input from fault-based PSHA: Remarks after the 2016 Central Italy earthquake sequence, AGU 100: Advancing Earth and Space Science
- [25] Valentini A, Visini F, and Pace B 2017 Integrating faults and past earthquakes into a probabilistic seismic hazard model for peninsular Italy, *Natural Hazards and Earth System Sciences* 17 (11) 2017
- [31] Causse M, Dalguer L A and Mai P M 2013 Variability of dynamic source parameters inferred from kinematic models of past earthquakes, *Geophysical Journal International* 196 (3) 607
- [41] Pace B, Visini F, and Peruzza L 2016 FiSH: MATLAB tools to turn fault data into seismic-hazard models, *Seismological Research Letters* 872A 374
- [46] Luzi L, Lanzano G, Felicetta C, D'Amico M C, Russo E, Sgobba S, Pacor, F and ORFEUS Working Group 5 2020 Engineering Strong Motion Database (ESM) (Version 2.0), Istituto Nazionale di Geofisica e Vulcanologia (INGV)
- [49] Imbsen, R A 2007 Proposed AASHTO guide specifications for LRFD seismic bridge design: Subcommittee for seismic effects on bridges, Imbsen Consulting